



Enhancement of catalytic activity over TiO₂-modified Al₂O₃ and ZnO–Cr₂O₃ composite catalyst for hydrogen production via dimethyl ether steam reforming

Mei Yang^{a,b}, Yong Men^a, Shulian Li^a, Guangwen Chen^{a,*}

^a Dalian National Laboratory for Clean Energy, Dalian Institute of Chemical Physics, Chinese Academy of Sciences, Dalian 116023, China

^b Graduate University, Chinese Academy of Sciences, Beijing 100049, China

ARTICLE INFO

Article history:

Received 30 January 2012

Received in revised form 26 April 2012

Accepted 27 April 2012

Available online 4 May 2012

Keywords:

Dimethyl ether

Steam reforming

Activity enhancement

H₂ production

ZnO–Cr₂O₃

TiO₂–Al₂O₃

ABSTRACT

The dimethyl ether steam reforming (DME SR) was carried out over the composite catalyst of ZnO–Cr₂O₃ coupled with Al₂O₃, TiO₂ or TiO₂–Al₂O₃ in the microreactor. The results showed that the catalytic activities were greatly enhanced over the composite catalyst of ZnO–Cr₂O₃ combined with TiO₂–Al₂O₃ (ZnCr–TiAl) in comparison to those combined with Al₂O₃ or TiO₂ in DME SR. By evaluating the catalytic activity of solid acids in DME hydrolysis, it was proposed that the better performance of TiO₂–Al₂O₃ in DME hydrolysis contributed to the superior activity of ZnCr–TiAl in DME SR, indicating a higher DME hydrolysis activity favored DME SR. In view of the characterization of N₂ physisorption, scanning electron microscope, X-ray diffraction and NH₃ temperature-programmed desorption, the promotion effect of TiO₂ on both DME hydrolysis and steam reforming was discussed in terms of the modification effect of TiO₂ on the acid properties of Al₂O₃ surface. The acid strength or total acid amount was enhanced by the addition of different TiO₂ content. In the 150 h medium stability test, there was no obvious deactivation for ZnCr–TiAl catalyst with the H₂ production rate of 345 mol h⁻¹ kg_{cat}⁻¹ and the CO selectivity in the dry reformat remained below 6%. The characterization results of the used catalyst revealed that no change in the crystalline phase and size occurred on the spent catalyst.

© 2012 Elsevier B.V. All rights reserved.

1. Introduction

Proton exchange membrane fuel cells (PEMFCs) research and development has become a flourishing area in recent years, due to their stationary and mobile applications as clean and efficient power generators at a range of scales [1]. However, the commercialization of PEMFCs has been hindered by some difficulties, such as durability, cost and hydrogen storage and distribution. Therefore, one of the most promising solutions to provide hydrogen is on site hydrogen generation from hydrocarbon fuels. Dimethyl ether (DME) has been considered as one of the potential fuels due to various advantages, such as high H/C ratio, high energy density, innocuous nature and easy storage and transportation due to the similar physical properties to those of LPG and LNG [2–4]. In addition, the direct synthesis of DME from syngas has been proved to be feasible by many literatures [5]. Among the reformation technologies, DME steam reforming (DME SR) has been regarded as the most suitable process to obtain H₂-rich reformat for fuel cell application because of its higher hydrogen yield and lower selectivity to CO which is considered as the poison to Pt electrode of PEMFCs [6].

Generally, DME SR is a couple of two consecutive reactions: the hydrolysis of DME to methanol over a solid acid, and then

the steam reforming of methanol formed (MSR). Therefore, the overall process usually needs a hybrid catalyst consisting of dual sites of acid sites and MSR sites. So far, many catalysts have been developed for DME SR, which are usually in the form of the mechanical mixture of a solid acid and a MSR catalyst [7–10]. Various solid acids, such as zeolite, WO₃–ZrO₂ and γ-Al₂O₃ are reported to be active for DME hydrolysis, while Cu-based catalysts are the common MSR catalysts. When zeolite and WO₃–ZrO₂ are coupled with Cu-based catalysts, DME SR can proceed below 300 °C because of the existence of strong Brønsted acid. Nevertheless, these composite catalysts are prone to deactivation due to the coke deposition [11,12]. Kawabata et al. suggested that the formation of coke materials was originated from the polymethyl aromatics produced by polymerization on the solid acid catalyst, followed by the migration to the Cu-based catalyst [8]. Compared with zeolite and WO₃–ZrO₂, γ-Al₂O₃ with weaker acid sites has been reported to be more durable for DME hydrolysis, but a relatively higher temperature between 350 and 500 °C is required for efficient hydrolysis of DME. Many studies have employed γ-Al₂O₃ as the solid acid in the reforming process, such as Al₂O₃ + Cu₂Mn₁Fe₃ [10], 2Cu–1Ni–17Al₂O₃ [13], Cu 20%/γ-Al₂O₃ [14] and particularly CuFe₂O₄ + Al₂O₃ [15]. Faungnawakij et al. found that CuFe₂O₄ + Al₂O₃ catalyst exhibited good activity and stability in DME SR at the temperature range of 350–450 °C. The high dispersion of metallic copper in the matrix of iron oxides reduced from spinel structure and their strong chemical interaction were

* Corresponding author. Tel.: +86 411 84379301; fax: +86 411 84379327.
E-mail address: gwchen@dicp.ac.cn (G. Chen).

attributed to the excellent performance [16,17]. In addition, the composite catalyst of noble metal-based catalyst coupled with a solid acid is another interesting catalytic system [18,19]. Ledesma et al. investigated the activity of Pd-based catalytic monoliths for DME SR. The best catalytic performance was obtained over Pd–ZrO₂ catalytic monolith and the interaction between Pd particles and the support may be the key factor in determining the catalytic performance [19]. Although good activity and low CO selectivity are obtained over Cu-based and noble metal-based catalysts in DME SR, the pyrophoric property and easy agglomeration at elevated temperature of Cu-based catalysts, and the high cost of noble metal-based catalysts cannot be ignored. Apart from Cu-based and noble metal-based catalysts, metal oxide catalysts have also attracted much attention for the advantages such as easy preparation, no pre-reduction and low cost. Mathew et al. found that Ca₂O₃ and Ga₂O₃ containing Al₂O₃ mixed oxide exhibited good activity in DME SR [20,21].

As mentioned above, the active temperature of the composite catalyst of an MSR catalyst combined with γ -Al₂O₃ is above 350 °C, which seems too high to supply H₂ for PEMFCs. Actually, by using an efficient heat exchanger such as a microchannel heat exchanger or a microchannel reactor integrated with microchannel heat exchanger structure, energy can be recovered between the feed and H₂-rich reformat gas. DME SR over the composite catalyst containing γ -Al₂O₃ can be integrated with Pd membrane reactor, whose operating temperature should be higher than 300 °C to avoid the Pd-H phase transition, to produce pure H₂. In addition, high-temperature proton exchange membrane fuel cells (HT-PEMFCs) have attracted much attention [22,23]. HT-PEMFCs operated between 100 and 200 °C can offer many advantages, such as high CO tolerance and easy integration of reformer technology. Li et al. [24] found the CO tolerance was 3% CO in H₂ at 200 °C, while that was 0.1% CO in H₂ at 125 °C. As a result, DME SR over the composite catalyst containing γ -Al₂O₃ can also be integrated with HT-PEMFCs.

In our previous work, ZnO–Cr₂O₃ was found to be an effective MSR catalyst between 400 and 500 °C [25]. In the same temperature range, γ -Al₂O₃ can effectively catalyze DME hydrolysis to methanol. Therefore, ZnO–Cr₂O₃ and γ -Al₂O₃ were selected as the reforming and hydrolyzing component for DME SR in the present study. Since DME hydrolysis is always considered to be the limiting step in DME SR, the enhancement in DME hydrolysis may bring about an increasing DME conversion. It is well documented that DME hydrolysis is influenced significantly by the amount and distribution of acid sites [26,27]. Thus, it is anticipated that the performance of γ -Al₂O₃ in DME hydrolysis can be improved by tuning the acid properties. According to the literature, the surface acid properties of γ -Al₂O₃ can be modified by the addition of TiO₂ in terms of the amount and strength of the acid sites [28,29]. Consequently, in this paper, we examined the performance of the composite catalyst of ZnO–Cr₂O₃ coupled with γ -Al₂O₃ and focused our attentions on the promotion effect of TiO₂ on the catalytic activity in the reforming process. In addition, ZnCr–TiAl catalyst was also evaluated in a parameter study varying the weight ratio of ZnO–Cr₂O₃ to TiO₂–Al₂O₃, gas hourly space velocity (GHSV) and molar ratio of water to DME (H₂O/DME).

2. Experimental

2.1. Catalyst preparation

ZnO–Cr₂O₃ was prepared by a co-precipitation method at a constant pH of 7–8. The metal nitrates [Zn(NO₃)₂·6H₂O, Cr(NO₃)₃·9H₂O] were dissolved into 200 ml de-ionized water. The aqueous solution of metal nitrates with a total cation concentration

of 1.0 M was contacted with a basic solution of aqueous ammonium at a stoichiometric molar ratio. The process was carried out by drop-wise addition of both solutions into a stirred flask containing 200 ml de-ionized water at 60 °C. The precipitate formed was aged in the mother liquid for 1 h, then removed, washed with de-ionized water several times and centrifuged. The obtained ZnO–Cr₂O₃ deposit was dried at 110 °C for 8 h and calcined at 500 °C for 3 h in air. The optimal Cr₂O₃ composition was 17.6 wt% [30].

TiO₂–Al₂O₃ was prepared as the following steps. First, dry powder of AlOOH (Shandong Alumina Company) was calcined at 500 °C for 4 h to prepare γ -Al₂O₃. Second, γ -Al₂O₃ powder was diluted and mixed well with 100 ml de-ionized water in a stirred flask. Then, Ti(SO₄)₂ aqueous solution and aqueous ammonium were added simultaneously into the flask at a constant pH of 7–8. The precipitate generated was washed with de-ionized water many times to eliminate SO₄²⁻ and centrifuged. The obtained TiO₂–Al₂O₃ deposit was dried at 110 °C for 8 h and calcined at 500 °C for 3 h in air.

The composite catalysts of ZnO–Cr₂O₃ and TiO₂–Al₂O₃ were prepared by mechanical milling in a mortar at desired weight ratios, and then calcined at 500 °C for 3 h. Subsequently, the catalysts were grounded, pressed, crushed and screened to 40–60 mesh (0.245–0.35 mm). The resultant samples were designated as ZnCr–XTiAl = Y, in which the symbol X and Y represented the weight ratio of TiO₂ to TiO₂–Al₂O₃ and ZnO–Cr₂O₃ to TiO₂–Al₂O₃, respectively.

2.2. Catalyst characterization

The specific surface area was measured by the BET method on a Quantachrome NOVA 4200e instrument using nitrogen adsorption isotherms at 77 K.

The morphology of the catalysts was observed by scanning electron microscope (JSM-6360 LV, JEOL).

The X-ray diffraction (XRD) pattern was obtained with a PANalytical X'Pert-Pro powder X-ray diffractometer, using Cu K α monochromatized radiation (λ = 0.1541 nm) at a scan speed of 5°/min.

Temperature programmed desorption of NH₃ (NH₃-TPD) was performed on a Micromeritics AutoChem 2920 apparatus. The amount of 200 mg catalyst was placed into a quartz U tube, heated for 2 h at 450 °C in Ar, and then kept at 100 °C for NH₃ adsorption. When saturated adsorption was achieved, the system was swept by He for 3 h. Then the temperature was programmed to increase to 450 °C under the heating rate of 10 °C/min. The desorbed NH₃ was analyzed by a TCD detector.

2.3. Catalytic test

DME SR was carried out in a multichannel microreactor under atmospheric pressure. The microreactor had 10 parallel channels with a width of 1.5 mm, a depth of 1.5 mm and a length of 40 mm. 800 mg catalyst particles with the size of 40–60 mesh were packed within the channels.

A mixture of DME, N₂ and water was purveyed into the vaporizer at 280 °C. The vapor was then fed into the microreactor. Subsequently, the reactor effluent passed through a condenser with a mixture of ice-water to trap the unreacted water and methanol. The flow rate of the dry reformat was measured by a soap bubble flow meter. The composition of the dry reformat was analyzed by an on-line gas chromatograph (GC 4000A, Beijing East & West Analytical Instruments Inc.) equipped with a thermal conductivity detector (TCD) and flame ionization detector (FID). A carbon molecular sieve column (TDX-01) was used to separate H₂, N₂, CO, CH₄ and CO₂ and a column of GDX-104 was used to detect DME. All data were collected when the catalytic activity was kept stable, and material balance on N₂ was calculated to verify the measurement accuracy.

Table 1
The BET surface area and total acid amount of the samples. \bar{p} .

Sample	Weight ratio of ZnO–Cr ₂ O ₃ to solid acid	BET surface area (m ² /g)	Acid amount (μmol/g)
Al ₂ O ₃	–	220	394
3% TiO ₂ –Al ₂ O ₃	–	182	396
10% TiO ₂ –Al ₂ O ₃	–	190	444
TiO ₂	–	79	362
ZnO–Cr ₂ O ₃	–	24	–
ZnCr–Al = 2:1	2:1	86	–
ZnCr–3% TiAl = 2:1	2:1	77	–
ZnCr–10% TiAl = 2:1	2:1	78	–
ZnCr–Ti = 2:1	2:1	34	–
ZnCr–10% TiAl = 4:1	4:1	52	–
ZnCr–10% TiAl = 1:3	1:3	151	–

The unreacted methanol in the condensate was found to be very low by an off-line chromatograph (GC 960, Shanghai HaiXin Analytical Instruments Inc.) equipped with a TCD, and could be ignored. The carbon balance for the samples investigated was between 0.97 and 1.03.

In this paper, GHSV, the conversion of DME which is transformed to H₂ (X_{DME}), CO selectivity (S_{CO}), CO₂ selectivity (S_{CO_2}), CH₄ selectivity (S_{CH_4}) in the dry reformat and H₂ space time yield (Y_{H_2}) are defined as follows:

$$GHSV = \frac{Q_{DME} + Q_{H_2O}}{V_R} \times 60 \quad (1)$$

$$X_{DME} = \frac{n_{CO} + n_{CO_2} + n_{CH_4}}{2n_{DME,0}} \times 100 \quad (2)$$

$$S_{CO} = \frac{n_{CO}}{n_{CO} + n_{CO_2} + n_{CH_4}} \times 100 \quad (3)$$

$$S_{CO_2} = \frac{n_{CO_2}}{n_{CO} + n_{CO_2} + n_{CH_4}} \times 100 \quad (4)$$

$$S_{CH_4} = \frac{n_{CH_4}}{n_{CO} + n_{CO_2} + n_{CH_4}} \times 100 \quad (5)$$

$$Y_{H_2} = \frac{n_{H_2}}{m_{cat}} \times 60 \quad (6)$$

where Q_{DME} and Q_{H_2O} are the volume flow rate of DME and water under the conditions of 1 atm and 25 °C (ml min⁻¹); V_R is the volume of packed catalyst bed (ml); n_{CO} , n_{CO_2} , n_{CH_4} and n_{H_2} are the molar flow rate of CO, CO₂, CH₄ and H₂ in the dry reformat (mol min⁻¹); $n_{DME,0}$ is the molar flow rate of DME in the feed (mol min⁻¹); m_{cat} is the weight of the catalyst (kg).

3. Results and discussion

3.1. Catalyst characterization

3.1.1. BET surface area

The results from the BET measurements are summarized in Table 1. The surface area of Al₂O₃ and TiO₂ is 220 and 79 m²/g, respectively. Introducing doping TiO₂ onto Al₂O₃ results in an obvious decrease in the surface area, which is in accordance with César et al.'s result [31]. The surface area of 3% TiO₂–Al₂O₃ is comparable with that of 10% TiO₂–Al₂O₃. ZnO–Cr₂O₃ maintains the smallest surface area of 24 m²/g among all of the samples. Therefore, the surface area of the composite catalyst is much lower than that of the solid acid (Al₂O₃, TiO₂–Al₂O₃ or TiO₂). The surface area of ZnCr–Al = 2:1, ZnCr–3% TiAl = 2:1 and ZnCr–10% TiAl = 2:1 is 86, 77 and 78 m²/g, respectively. In addition, it is evident that the surface area of the composite catalyst decreases with the increasing weight ratio of ZnO–Cr₂O₃ to TiO₂–Al₂O₃.

3.1.2. SEM

According to the literature, inter-particle diffusion between the solid acid and MSR catalyst influences the catalytic activity significantly in DME SR, and thereby, the mixing state of the solid acid and MSR catalyst is an important factor for getting a high activity [32]. Faungnawakij et al. found that a well-mixed composite catalyst of CuFe₂O₄ coupled with Al₂O₃ exhibited the best catalytic performance in DME SR, in comparison with the catalysts placed randomly or separately [32]. As a result, ZnO–Cr₂O₃ and TiO₂–Al₂O₃ were mechanically mixed together in a mortar firstly. Fig. 1 presents the SEM images of ZnO–Cr₂O₃, 10% TiO₂–Al₂O₃ and ZnCr–10% TiAl = 2:1. As shown in Fig. 1, the composite catalyst shows a close contact of ZnO–Cr₂O₃ and TiO₂–Al₂O₃. It indicates that a well-mixed state can be achieved by the mechanically mixing in a mortar, which is a prerequisite for a high DME conversion.

3.1.3. XRD

Fig. 2a shows the XRD patterns of TiO₂–Al₂O₃ calcined at 500 °C for 3 h. Anatase phase is identified in TiO₂. The XRD pattern of Al₂O₃ shows three broad peaks at $2\theta = 37.5^\circ$, 45.5° and 66.8° , indicating a poor crystallinity of γ -Al₂O₃. Diffraction characteristic peaks of anatase cannot be observed by XRD in 3% TiO₂–Al₂O₃. This indicates that TiO₂ is uniformly dispersed on the surface or intruded into the body phase of Al₂O₃, thus resulting in a decrease in the specific surface area of the doped catalyst. The characteristic peaks of anatase can be detected in XRD patterns as the weight ratio of TiO₂ is 10 wt%, suggesting that the amount of dopant exceeds the largest capacity of the monolayer distribution on Al₂O₃. These results can be explained by the incorporation model proposed by Chen et al. [33]. The incorporation model suggests that the dispersed metal cations are incorporated into the surface vacant sites of the support with their accompanying anions sitting on the top for extra charge compensation, resulting in the formation of M–O–M' linkages. Generally, the dispersion capacity of metal compounds is determined by the structure of support and the shielding effect of the capping anions. In the case of TiO₂–Al₂O₃ system, at the low TiO₂ loading (≤ 0.56 mmol, 100 m⁻² γ -Al₂O₃), the Ti⁴⁺ ions are proposed to be incorporated into the surface octahedral vacancy of Al₂O₃, accompanied by two oxygen anions associated with the Ti⁴⁺ ion on the top of the occupied site forming capping oxygen [34]. This type of linkage has been proven to exist in many literatures [28,35,36]. For example, Pophal et al. found that the IR spectra corresponding to hydroxyl stretching vibrations of Al–OH groups faded with the increasing TiO₂ content, indicating the formation of Al–O–Ti linkage [37]. A further increase in the loading of TiO₂ results in the formation of crystalline TiO₂. Therefore, on the basis of the incorporation model, the Ti⁴⁺ ions exist in the form of Ti–O–Al linkages in 3% TiO₂–Al₂O₃, whereas the Ti⁴⁺ ions also appear as Ti–O–Ti linkages in 10% TiO₂–Al₂O₃ besides Ti–O–Al linkages. In addition, it is evident that the peak line of anatase of 10% TiO₂–Al₂O₃ broadens in comparison with that of TiO₂, revealing a smaller mean crystalline size of anatase in 10% TiO₂–Al₂O₃, according to Scherrer's equation. The crystalline size of anatase is 7 and 15 nm in 10% TiO₂–Al₂O₃ and TiO₂, respectively.

Fig. 2b displays the XRD patterns of ZnCr–TiAl composite catalysts with different TiO₂ contents. Two crystalline phases of ZnO and ZnCr₂O₄ are detected in all of the XRD patterns. γ -Al₂O₃ is identified in all of the samples except ZnCr–Ti = 2:1. In the case of ZnCr–10% TiAl = 2:1 and ZnCr–Ti = 2:1, the characteristic peak of anatase can be observed at $2\theta = 25.3^\circ$. Fig. 2c shows the XRD patterns of ZnO–Cr₂O₃ to 10% TiO₂–Al₂O₃. In evidence, the intensity of the XRD peaks corresponding to ZnO and ZnCr₂O₄ becomes more obvious with the increasing weight ratio of ZnO–Cr₂O₃ to TiO₂–Al₂O₃, whereas that corresponding to Al₂O₃ and TiO₂ becomes lower.

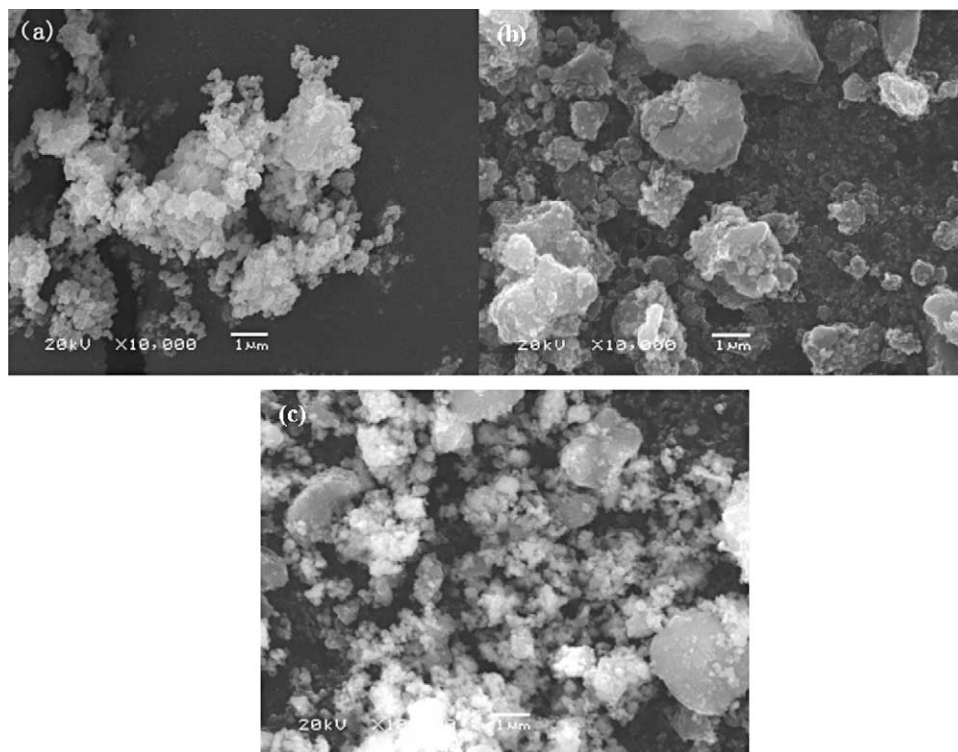


Fig. 1. The SEM images of (a) ZnO–Cr₂O₃, (b) 10% TiO₂–Al₂O₃, and (c) ZnCr–10% TiAl=2:1.

3.1.4. NH₃-TPD

TiO₂–Al₂O₃ samples with varying TiO₂ contents have been studied by a number of investigations with respect to their physicochemical properties. Based on the pyridine adsorption IR results, only Lewis acid sites are observed in Al₂O₃ and TiO₂–Al₂O₃ (Al₂O₃ as the host oxide) [29,38]. Typically, Lewis acid sites can serve as the active sites for DME hydrolysis. In this paper, NH₃-TPD was employed to estimate the amount and strength of acid sites formed on the catalyst surface. The NH₃-TPD patterns of TiO₂, TiO₂–Al₂O₃ and Al₂O₃ are plotted in Fig. 3. As shown in Fig. 3, the uptake pattern of Al₂O₃ has two distinct regions 1 and 2, from 100 to 350 °C (type I) and 350 to 450 °C (type II), respectively. TiO₂ displays a broad peak originated from 100 to 450 °C. 3% TiO₂–Al₂O₃ and 10% TiO₂–Al₂O₃ show similar NH₃ desorption pattern with Al₂O₃. It is interesting to note that when Al₂O₃ is doped with 3% TiO₂, the desorption peak of type II acid sites shifts from 360 °C to 410 °C. It is well-known that the acid sites corresponding to the low/high temperature peak are referred to the weak/strong acid sites. Therefore, it can be concluded that 3% TiO₂–Al₂O₃ has stronger type II acid sites than Al₂O₃. It has been observed that the binary metal oxides often display increased acidity over their pure counterparts [39,40]. The increase in acidity is ascribed to the distribution of an excess negative/positive charge caused by the formation of bridged hetero metal–oxygen bonds, as suggested by Tanabe's model [41]. On the basis of the XRD results, the titanium ions may be bonded mainly via oxygen bridges to aluminium ions in 3% TiO₂–Al₂O₃. Hence, the enhanced strength of type II acid sites of 3% TiO₂–Al₂O₃ can be attributed to the possible formation of Ti–O–Al bonds. This kind of heterolinkage has been proposed in many literatures to enhance the acidity in TiO₂–Al₂O₃ systems [28,42]. When the TiO₂ composition goes up to 10%, the peak temperature of type II acid sites returns to ca. 360 °C. As mentioned above, the crystalline anatase is found at higher titanium content (10% TiO₂–Al₂O₃), implying the presence of Ti–O–Ti bonds. As a consequence, the shift of the desorption peak of type II acid sites may be ascribed to the segregation of anatase. Though the acid strength of 10% TiO₂–Al₂O₃

is analogous with that of Al₂O₃, it possesses a higher acid amount as compared with other samples (Table 1). Taking the BET surface area into account, the acid density of Al₂O₃ and TiO₂ is 1.8 and 4.6 µmol/m², respectively. Hence, the increase in the acid amount of 10% TiO₂–Al₂O₃ may be partly contributed by the dispersed TiO₂ on Al₂O₃.

3.2. Catalytic activity for DME hydrolysis and SR

3.2.1. DME hydrolysis over TiO₂–Al₂O₃ samples

It is well known that DME hydrolysis can always be catalyzed by solid acids, and the composite catalysts using the different solid acids with the same MSR catalyst show dissimilar activity in DME SR. Hence, we investigated the catalytic activity of TiO₂–Al₂O₃ samples for DME hydrolysis firstly. Fig. 4 shows the results of DME hydrolysis over TiO₂–Al₂O₃ samples. It can be seen that the DME conversion increases with the increasing reaction temperature over all samples investigated. TiO₂ exhibits a low activity towards DME hydrolysis over the entire temperature range. In comparison, the DME conversion over Al₂O₃ is much higher than that on TiO₂, and the DME conversion coincides with the equilibrium value at 420 °C. The addition of TiO₂ to Al₂O₃ is found to significantly improve the DME hydrolysis. For instance, 3% TiO₂ doping gives rise to a remarkable increase in the catalytic activity of Al₂O₃, and the DME conversion approaches to the equilibrium value at 380 °C. The DME conversion over 10% TiO₂–Al₂O₃ is comparable with that over 3% TiO₂–Al₂O₃.

According to the literature, TiO₂–Al₂O₃ as a catalyst support for metal has been widely used for the decomposition of perchloroethylene [43], hydrodesulfurization [44] and CO oxidation [45], etc. TiO₂–Al₂O₃ can be prepared by various methods, such as coprecipitation, sol–gel, chemical vapor deposition and impregnation. Many reports revealed that metal supported on TiO₂–Al₂O₃, such as Ag [29], Mo [46] and Cr [43], showed superior catalytic activity than that supported on TiO₂ or Al₂O₃. This activity enhancement was usually correlated with the physicochemical properties

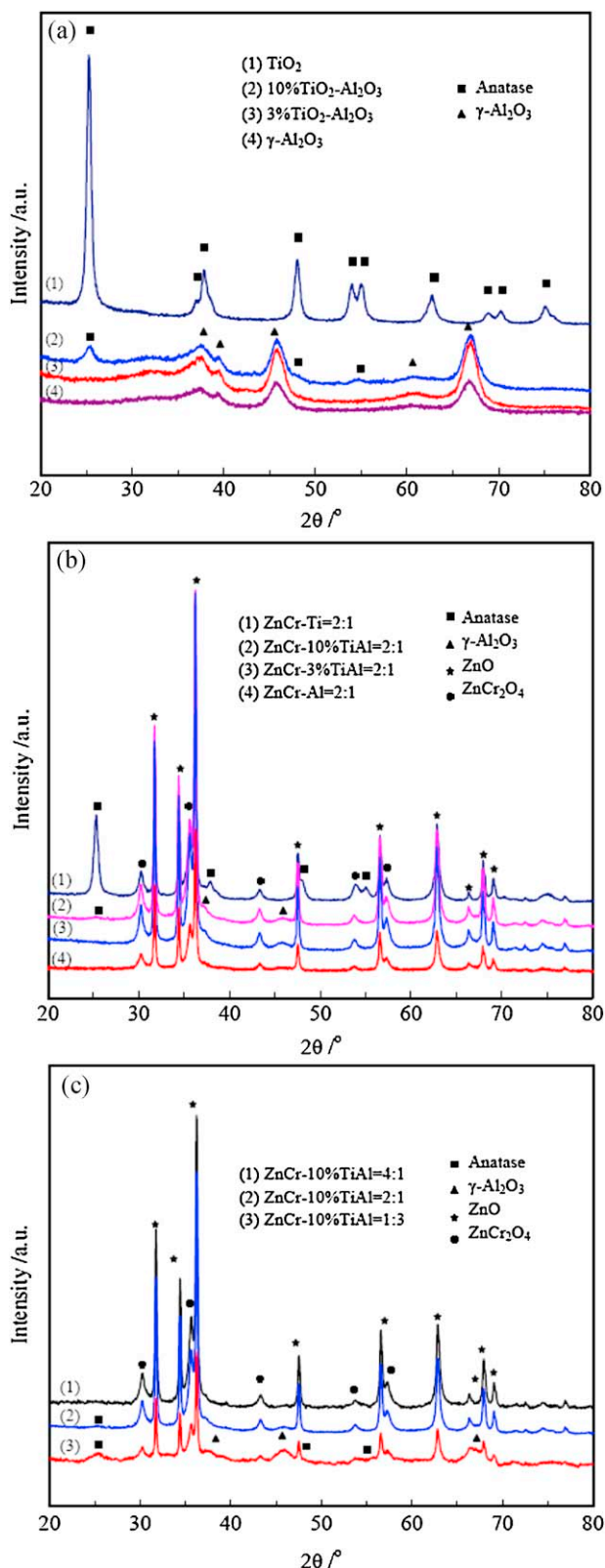


Fig. 2. The XRD patterns of (a) $\text{TiO}_2\text{-Al}_2\text{O}_3$, (b) ZnCr-TiAl composite catalysts with different TiO_2 contents, and (c) ZnCr-TiAl composite catalysts with different weight ratio of ZnO-Cr $_2$ O $_3$ to $\text{TiO}_2\text{-Al}_2\text{O}_3$.

of $\text{TiO}_2\text{-Al}_2\text{O}_3$, which are different from TiO_2 and Al_2O_3 , including surface area, acid properties and the interaction between the support with metal. Besides acting as a support, $\text{TiO}_2\text{-Al}_2\text{O}_3$ itself can catalyze the dehydration of methanol to DME. In comparison

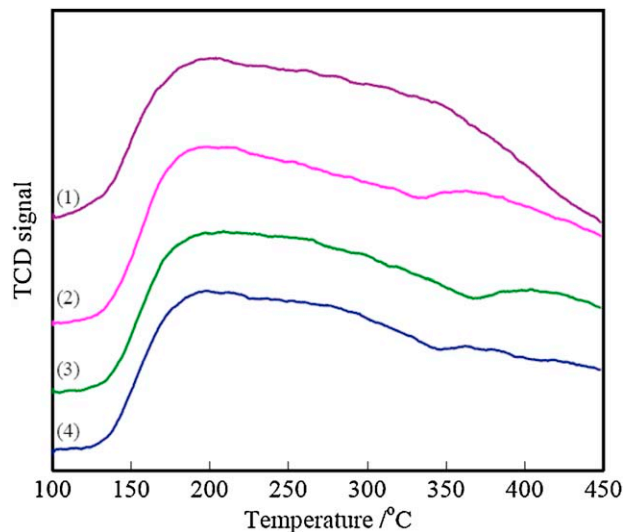


Fig. 3. The NH_3 -TPD profiles of (1) TiO_2 , (2) 10% $\text{TiO}_2\text{-Al}_2\text{O}_3$, (3) 3% $\text{TiO}_2\text{-Al}_2\text{O}_3$, and (4) Al_2O_3 .

with Al_2O_3 , the TiO_2 -modified Al_2O_3 ($\text{TiO}_2 \leq 10$ wt%) showed higher catalytic activity and DME selectivity, probably because of an enhanced Lewis acidity of $\text{TiO}_2\text{-Al}_2\text{O}_3$ [28]. In the present work, TiO_2 , $\text{TiO}_2\text{-Al}_2\text{O}_3$ and Al_2O_3 present distinct performance in DME hydrolysis. The catalytic activity of TiO_2 is much lower than Al_2O_3 . This is probably due to the lowest surface area and acid amount of TiO_2 . 3% $\text{TiO}_2\text{-Al}_2\text{O}_3$ and 10% $\text{TiO}_2\text{-Al}_2\text{O}_3$, the most active samples, possess the lower surface area than Al_2O_3 . This indicates that there is no clear correlation between the surface area and the catalytic activity. Faungnawakij et al. found that DME hydrolysis can be enhanced by a higher acid amount and stronger acid strength [26]. With respect to the NH_3 -TPD results, the addition of TiO_2 can tune the surface acid properties of Al_2O_3 . The type II acid sites are strengthened in 3% $\text{TiO}_2\text{-Al}_2\text{O}_3$, whereas a higher acid amount is obtained in 10% $\text{TiO}_2\text{-Al}_2\text{O}_3$. Both changes in acid properties are the essential reasons for the higher activity for DME hydrolysis.

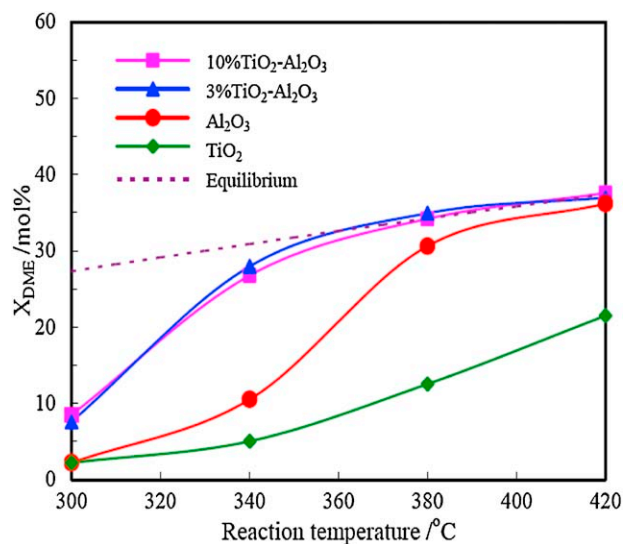


Fig. 4. The DME conversion as a function of reaction temperature in DME hydrolysis. $\text{GHSV} = 7900 \text{ h}^{-1}$; $\text{H}_2\text{O}/\text{DME} = 4.8$.

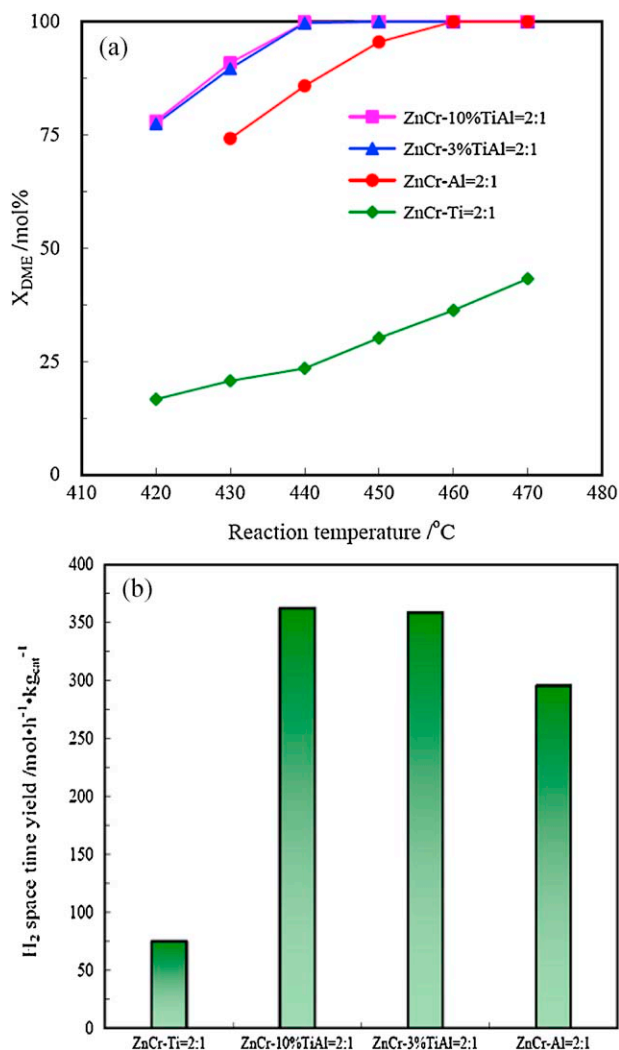


Fig. 5. (a) DME conversion as a function of reaction temperature and (b) H₂ space time yield over ZnCr–TiAl catalysts in DME SR, reaction temperature = 430 °C. GHSV = 7900 h⁻¹; H₂O/DME = 4.8.

3.2.2. DME SR over ZnCr–TiAl catalysts with different TiO₂ contents

DME SR was carried out over ZnCr–TiAl composite catalysts. The experiments were operated under the reaction conditions of H₂O/DME = 4.8 and GHSV = 7900 h⁻¹. Fig. 5a illustrates the DME conversion as a function of reaction temperature over ZnCr–TiAl catalysts with different TiO₂ contents. It can be seen that the catalytic activity of every composite catalyst increases with the reaction temperature. ZnO–Cr₂O₃ exhibits low activity for DME SR (<2%), probably due to the lack of acid sites in the catalyst. The conversion of DME is greatly enhanced by the addition of any of the acid components. In addition, all TiO₂ doped catalysts perform better than the un-doped one. ZnCr–3% TiAl and ZnCr–10% TiAl show the highest DME conversion. For example, the DME conversion on ZnCr–3% TiAl = 2:1 and ZnCr–10% TiAl = 2:1 is 91% at 430 °C, whereas that on ZnCr–Al = 2:1 and ZnCr–Ti = 2:1 is 74% and 21%, respectively. The catalytic activity follows the order ZnCr–3% TiAl = 2:1 ≈ ZnCr–10% TiAl = 2:1 > ZnCr–Al = 2:1 > ZnCr–Ti = 2:1, in good agreement with the order with respect to the DME conversion in DME hydrolysis. It seems that the catalytic behavior of the composite catalysts for the reforming of DME is closely related to the catalytic behavior of the corresponding acid components for DME hydrolysis. In other words, the composite catalyst combined ZnO–Cr₂O₃ with the solid acid which performs better in DME

hydrolysis shows superior activity in DME SR. Fig. 5b shows the H₂ space time yield over different composite catalysts at 430 °C. The H₂ space time yield exhibits the same order with the DME conversion. The H₂ space time yield over ZnCr–3% TiAl = 2:1 and ZnCr–10% TiAl = 2:1 is higher than that over ZnCr–Ti = 2:1 and ZnCr–Al = 2:1.

The CO, CO₂ and CH₄ selectivity are plotted in Fig. 6 as a function of the reaction temperature. It is evident that CO selectivity increases with the increasing reaction temperature, whereas CO₂ selectivity goes to the opposite direction. In addition, the composite catalyst with higher activity in DME SR is found to possess higher CO selectivity. In the case of ZnCr–3% TiAl = 2:1 and ZnCr–10% TiAl = 2:1, the CO selectivity is ca. 7% with a full DME conversion at 440 °C. The route of CO formation will be discussed in the Section 3.2.3.2. The samples with TiO₂ are found to generate CH₄ with the selectivity ranging from 0.15 to 0.5%, whereas CH₄ is not formed over ZnCr–Al = 2:1. This result indicates that the formation of CH₄ may be associated with the presence of TiO₂. Generally, CH₄ is likely to originate from the direct decomposition of DME (CH₃OCH₃ → H₂ + CO + CH₄). DME decomposes into methyl (CH₃-) and methoxy (CH₃O-) species, and the methyl can easily be further hydrogenated to form methane. Hussein et al. reported that dimethyl ether can react over TiO₂ surface to form CH₄ at a higher temperature than 350 °C [47].

3.2.3. The effect of the weight ratio of ZnO–Cr₂O₃ to TiO₂–Al₂O₃ and operation conditions

3.2.3.1. The weight ratio of ZnO–Cr₂O₃ to TiO₂–Al₂O₃. The effect of the weight ratio of ZnO–Cr₂O₃ to 10% TiO₂–Al₂O₃ on the catalytic activity was investigated. Generally speaking, DME hydrolysis is a thermodynamically limited reaction. For instance, the equilibrium conversion of DME is ca. 37.4% at 420 °C (H₂O/DME = 4.8). If the produced methanol is subsequently transformed to H₂ and CO₂, the equilibrium for DME hydrolysis will shift to the right, resulting in a higher DME conversion. Therefore, the weight balance of ZnO–Cr₂O₃ and TiO₂–Al₂O₃ for composite catalyst is a key factor to obtain a high DME conversion. In this section, the weight ratio of ZnO–Cr₂O₃ to 10% TiO₂–Al₂O₃ was varied from 4:1 to 1:3. Fig. 7 shows the DME conversion and CO selectivity as a function of the reaction temperature over the composite catalyst with different weight ratio of ZnO–Cr₂O₃ to 10% TiO₂–Al₂O₃. Commonly, solid acid-rich samples give rise to a shortage of active sites for MSR, leading to a low DME conversion. Hence, the activity of ZnCr–10% TiAl = 1:3 is less than that of ZnCr–10% TiAl = 2:1 (as shown in Fig. 7). The best performance is obtained over ZnCr–10% TiAl = 2:1, indicating a proper balance between the MSR sites and acid sites in this sample. As the weight ratio of ZnO–Cr₂O₃ to 10% TiO₂–Al₂O₃ further increases to 4:1, the activity goes down due to the lack of acid sites. To sum up, the optimal weight ratio is determined to be 2:1. On the other side, the CO selectivity seems to be much less affected by the weight ratio of ZnO–Cr₂O₃ to 10% TiO₂–Al₂O₃.

3.2.3.2. GHSV. The DME conversion and the CO selectivity are plotted in Fig. 8 as a function of GHSV. The experiments were performed under the reaction conditions of 420 °C and H₂O/DME = 4.8. As shown in Fig. 8, the DME conversion decreases from 79.6% to 29.1% as the GHSV increases from 7900 to 36,520 h⁻¹. This is caused by the decreasing contact time between the reactant and the catalyst bed.

The desired DME SR is to produce hydrogen by the dehydrogenation of oxygenate species to produce as much as CO₂. Meanwhile, CO is inevitably formed in the reforming process, which is well-known as a poison to Pt electrode of PEMFCs. In order to inhibit the generation of CO in the reforming process, it is necessary to investigate the route of CO formation. As discussed above, the decomposition of DME occurs over ZnCr–TiAl composite catalysts. Therefore, according to CH₄ selectivity, CO selectivity brought

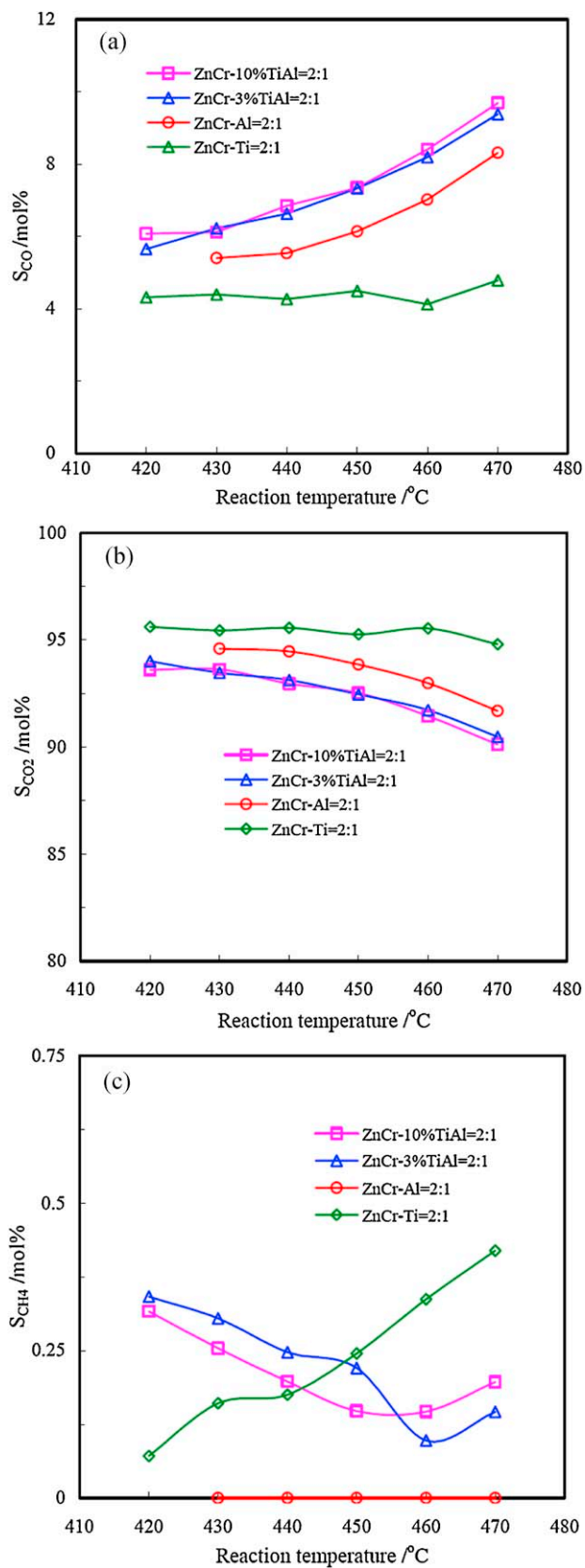


Fig. 6. (a) CO selectivity, (b) CO₂ selectivity, and (c) CH₄ selectivity as a function of reaction temperature in DME SR. GHSV = 7900 h⁻¹; H₂O/DME = 4.8.

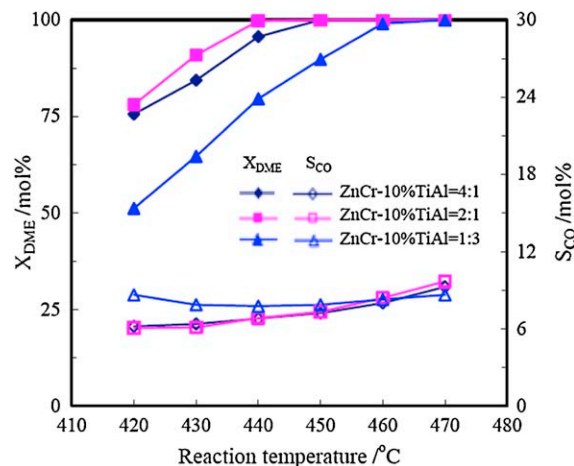


Fig. 7. DME conversion and CO selectivity over the composite catalysts with different weight ratio of ZnO–Cr₂O₃ to 10% TiO₂–Al₂O₃ in DME SR. GHSV = 7900 h⁻¹; H₂O/DME = 4.8.

about by DME decomposition is calculated to be 0.15–0.5%, which is much lower than the total CO selectivity. This implies that CO is mainly not generated by the decomposition of DME. Hence, the majority of by-product CO may be formed via MSR process. With respect to the literatures on the reaction mechanisms of MSR, CO is produced mainly via three pathways: (1) CO is an intermediate and formed directly through methanol decomposition (DM) followed by water gas shift reaction (WGS) [48]; (2) CO is produced by reverse water gas shift reaction (RWGS) as a secondary product [49]; (3) CO is generated directly from DM paralleled with MSR [50]. In this study, the CO concentration is far below its equilibrium value of WGS, indicating that mechanism 1 is not involved in the reaction pathway of CO formation. If CO is produced by mechanism 2, the CO selectivity will decrease with the increasing GHSV, whereas the CO selectivity is independent of GHSV in the mechanism 3. It is evident in Fig. 8 that the CO selectivity first declines gradually with increasing GHSV and then approaches a constant level when GHSV is larger than 24,000 h⁻¹. This indicates that RWGS and DM are both responsible for the CO formation.

3.2.3.3. H₂O/DME. The effect of the molar ratio of steam to dimethyl ether (H₂O/DME) on the DME conversion and CO selectivity was investigated over ZnCr–10% TiAl=2:1 catalyst. The

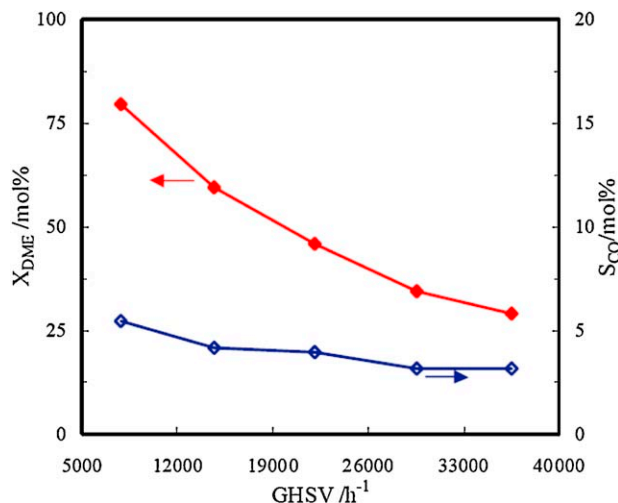


Fig. 8. DME conversion and CO selectivity as a function of GHSV over ZnCr–10% TiAl=2:1 in DME SR. Reaction temperature = 420 °C; H₂O/DME = 4.8.

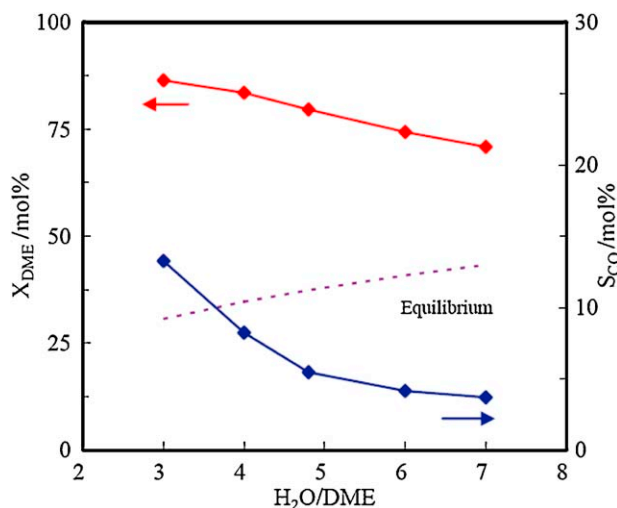


Fig. 9. DME conversion and CO selectivity as a function of $\text{H}_2\text{O}/\text{DME}$ ratio over $\text{ZnCr-10\% TiAl=2:1}$ in DME SR. Reaction temperature = 420°C ; $\text{GHSV} = 7900 \text{ h}^{-1}$.

experiments were carried out under the conditions of reaction temperature = 420°C . As stated in the introduction, DME SR consists of two consecutive reactions: DME hydrolysis and MSR. Accordingly, the effect of the rising $\text{H}_2\text{O}/\text{DME}$ ratio on DME SR exhibits in two-folds. On one hand, the rising water concentration can shift the thermodynamic equilibrium to the right, resulting in an improvement in DME hydrolysis equilibrium (as shown in Fig. 9). On the other hand, the increase in the $\text{H}_2\text{O}/\text{DME}$ ratio can reduce the reaction rate of MSR, brought about by the competitive adsorption of water and methanol on $\text{ZnO-Cr}_2\text{O}_3$ surface [51]. In this work, it is evident in Fig. 9 that DME conversion decreases with the increase in the $\text{H}_2\text{O}/\text{DME}$ ratio, corresponding to a decrease in the CO selectivity. The DME conversion and CO selectivity decrease from 86.4% to 70.9% and 13.3% to 3.7%, respectively, as the $\text{H}_2\text{O}/\text{DME}$ ratio increases from 3 to 7. As mentioned above, DME hydrolysis equilibrium is promoted by the rising water concentration, whereas MSR is restrained. Therefore, the decreasing DME conversion indicates that the increase in hydrolysis of DME cannot offset the activity loss in MSR. In addition, as mentioned above, CO is partly produced by RWGS. RWGS can be suppressed by the increasing water concentration, which is responsible for the decrease in CO selectivity.

3.2.4. The life time

Evaluating the preservation of the catalyst stability during a catalytic process is one of the most important goals for practical purposes. The time on stream study was performed using ZnCr-3\% TiAl=2:1 composite catalyst at 430°C , 7900 h^{-1} and $\text{H}_2\text{O}/\text{DME} = 4.8$, and the result is present in Fig. 10a. The result indicates that the catalytic activity, expressed in terms of DME conversion and H_2 production rate, shows no obvious deactivation for reaction time lasted for about 150 h. During the whole process, the CO and CH_4 selectivity in the dry gases is less than 6% and 0.34%, respectively. The moderate stability of the composite catalyst demonstrates the stable activity of $\text{TiO}_2\text{-Al}_2\text{O}_3$ for DME hydrolysis and $\text{ZnO-Cr}_2\text{O}_3$ for MSR. The results reported by Cao et al. showed that the long stability of $\text{ZnO-Cr}_2\text{O}_3$ for MSR was partly ascribed to the formation of ZnCr_2O_4 [30]. The XRD pattern of the used catalyst is reported in Fig. 10b. In comparison with the fresh catalyst, no change in the XRD patterns occurs on the used catalyst.

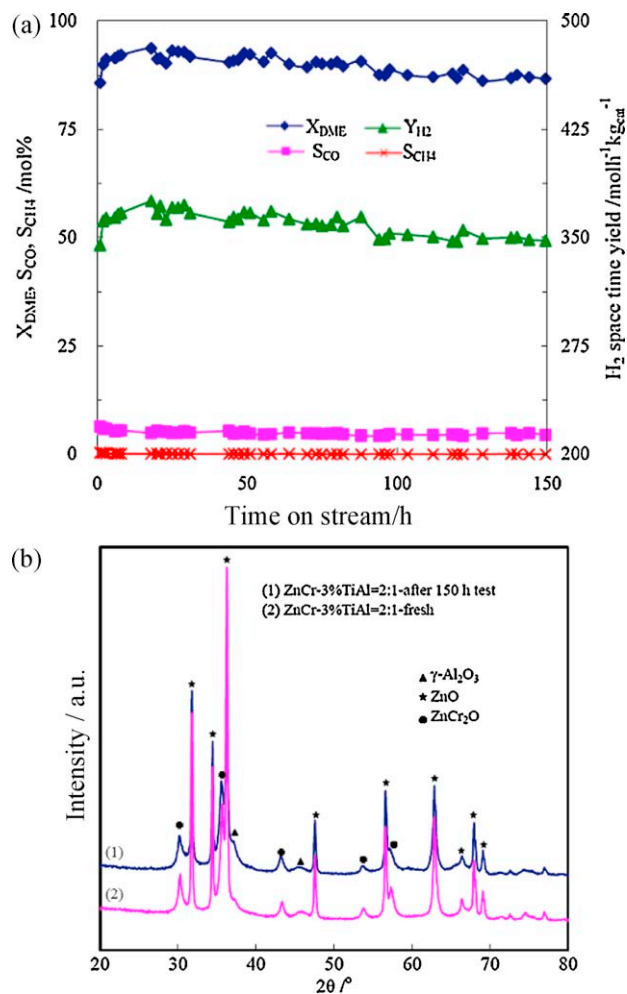


Fig. 10. (a) Stability test over ZnCr-3\% TiAl=2:1 catalyst, reaction temperature = 430°C , $\text{GHSV} = 7900 \text{ h}^{-1}$, $\text{H}_2\text{O}/\text{DME} = 4.8$. (b) The XRD pattern of spent ZnCr-3\% TiAl=2:1 .

4. Conclusion

This work has demonstrated that DME can be effectively reformed to hydrogen on the composite catalyst of $\text{ZnO-Cr}_2\text{O}_3$ coupled with Al_2O_3 or $\text{TiO}_2\text{-Al}_2\text{O}_3$. The most relevant conclusions of this work can be summarized as follows:

- (1) Compared with Al_2O_3 , the TiO_2 -deposited Al_2O_3 (3% or 10% TiO_2 loading) showed higher activity in DME hydrolysis. The $\text{NH}_3\text{-TPD}$ results revealed that the addition of TiO_2 can tune the acid amount and strength of Al_2O_3 . In the case of 3% $\text{TiO}_2\text{-Al}_2\text{O}_3$, the medium strong acid sites were strengthened due to the formation of Al-O-Ti linkages. For 10% $\text{TiO}_2\text{-Al}_2\text{O}_3$, the total acid amount was higher than any other sample, probably because of the dispersed TiO_2 on Al_2O_3 . Stronger acidity and higher total acid amount both favored DME hydrolysis.
- (2) Subsequently, a higher DME SR activity was observed over $\text{ZnO-Cr}_2\text{O}_3$ combined with 3% $\text{TiO}_2\text{-Al}_2\text{O}_3$ or 10% $\text{TiO}_2\text{-Al}_2\text{O}_3$. A good correlation between DME hydrolysis and SR activity revealed that a higher hydrolysis activity was beneficial to the reformation of DME to produce hydrogen. The optimal weight ratio of $\text{ZnO-Cr}_2\text{O}_3$ to 10% $\text{TiO}_2\text{-Al}_2\text{O}_3$ was ca. 2/1.
- (3) The DME conversion decreased with the increasing GHSV and molar ratio of H_2O to DME, accompanied by a decrease in CO selectivity. The results indicated that reverse water gas shift

reaction and methanol decomposition were both involved in the formation of CO.

- (4) During the 150 h test, there was no obvious deactivation over ZnCr–3% TiAl = 2:1. During the whole process, the CO and CH₄ selectivity in the dry gases was less than 6% and 0.34%, respectively. Considering the easy availability, no pre-reduction, low cost and medium stability at evaluated temperature of ZnCr–TiAl catalysts, the present catalyst system can serve as a potential metal oxide catalyst for DME SR.

Acknowledgements

The authors gratefully acknowledge the financial support from the Natural Science Foundation of Liaoning Province (No. 201102219), DICP 100-Talent Program, and the National Natural Science Foundation of China (No. 20906087).

References

- [1] T.E. Springer, T.A. Zawodzinski, S. Gottesfeld, *J. Electrochem. Soc.* 138 (1991) 2334–2342.
- [2] V.V. Galvita, G.L. Semin, V.D. Belyaev, T.M. Yurieva, V.A. Sobyenin, *Appl. Catal. A: Gen.* 216 (2001) 85–90.
- [3] Y. Yamada, T. Mathew, A. Ueda, H. Shioyama, T. Kobayashi, *Appl. Surf. Sci.* 252 (2006) 2593–2597.
- [4] K. Takeishi, H. Suzuki, *Appl. Catal. A: Gen.* 260 (2004) 111–117.
- [5] G.H. Yang, N. Tsubaki, J. Shamoto, Y. Yoneyama, Y. Zhang, *J. Am. Chem. Soc.* 132 (2010) 8129–8136.
- [6] J.J. Baschuk, X.G. Li, *Int. J. Energy Res.* 25 (2001) 695–713.
- [7] T. Matsumoto, T. Nishiguchi, H. Kanai, K. Utani, Y. Matsumura, S. Imamura, *Appl. Catal. A: Gen.* 276 (2004) 267–273.
- [8] T. Kawabata, H. Matsuoka, T. Shishido, D.L. Li, Y. Tian, T. Sano, K. Takehira, *Appl. Catal. A: Gen.* 308 (2006) 82–90.
- [9] K. Oka, T. Nishiguchi, H. Kanai, K. Utani, S. Imamura, *Appl. Catal. A: Gen.* 309 (2006) 187–191.
- [10] Y. Tanaka, R. Kikuchi, T. Takeguchi, K. Eguchi, *Appl. Catal. B* 57 (2005) 211–222.
- [11] T. Nishiguchi, K. Oka, T. Matsumoto, H. Kanai, K. Utani, S. Imamura, *Appl. Catal. A: Gen.* 301 (2006) 66–74.
- [12] N. Shimoda, K. Faungnawakij, R. Kikuchi, K. Eguchi, *Appl. Catal. A: Gen.* 378 (2010) 234–242.
- [13] X.L. Wang, X.M. Pan, R. Lin, S.Y. Kou, W.B. Zou, J.X. Ma, *Int. J. Hydrogen Energy* 35 (2010) 4060–4068.
- [14] S. Park, H. Kim, B. Choi, *Catal. Today* 164 (2011) 240–245.
- [15] K. Faungnawakij, Y. Tanaka, N. Shimoda, T. Fukunaga, R. Kikuchi, K. Eguchi, *Appl. Catal. B* 74 (2007) 144–151.
- [16] K. Faungnawakij, N. Shimoda, T. Fukunaga, R. Kikuchi, K. Eguchi, *Appl. Catal. B* 92 (2009) 341–350.
- [17] K. Faungnawakij, R. Kikuchi, T. Fukunaga, K. Eguchi, *Catal. Today* 138 (2008) 157–161.
- [18] A. Gazsi, I. Ugrai, F. Solymosi, *Appl. Catal. A: Gen.* 391 (2011) 360–366.
- [19] C. Ledesma, U.S. Ozkan, J. Llorca, *Appl. Catal. B* 101 (2011) 690–697.
- [20] T. Mathew, Y. Yamada, A. Ueda, H. Shioyama, T. Kobayashi, *Catal. Lett.* 100 (2005) 247–253.
- [21] T. Mathew, Y. Yamada, A. Ueda, H. Shioyama, T. Kobayashi, *Appl. Catal. A: Gen.* 286 (2005) 11–22.
- [22] F. Seland, T. Berning, B. Borresen, R. Tunold, *J. Power Sources* 160 (2006) 27–36.
- [23] A. Verma, K. Scott, *J. Solid State Electrochem.* 14 (2010) 213–219.
- [24] Q.F. Li, R.H. He, J.A. Gao, J.O. Jensen, N.J. Bjerrum, *J. Electrochem. Soc.* 150 (2003) A1599–A1605.
- [25] W.Q. Cao, G.W. Chen, S.L. Li, Q. Yuan, *Chem. Eng. J.* 119 (2006) 93–98.
- [26] K. Faungnawakij, Y. Tanaka, N. Shimoda, T. Fukunaga, S. Kawashima, R. Kikuchi, K. Eguchi, *Appl. Catal. A: Gen.* 304 (2006) 40–48.
- [27] T.A. Semelsberger, K.C. Ott, R.L. Borup, H.L. Greene, *Appl. Catal. B* 61 (2005) 281–287.
- [28] A. Khaleel, *Fuel* 90 (2011) 2422–2427.
- [29] J.H. Li, Y.Q. Zhu, R. Ke, J.M. Hao, *Appl. Catal. B* 80 (2008) 202–213.
- [30] W.Q. Cao, G.W. Chen, J.S. Chu, S.L. Li, Q. Yuan, *Chin. J. Catal.* 27 (2006) 895–898.
- [31] D.V. Cesar, R.F. Robertson, N.S. Resende, *Catal. Today* 133 (2008) 136–141.
- [32] K. Faungnawakij, N. Shimoda, N. Viriya-empikul, R. Kikuchi, K. Eguchi, *Appl. Catal. B* 97 (2010) 21–27.
- [33] Y. Chen, L.F. Zhang, *Catal. Lett.* 12 (1992) 51–62.
- [34] J. Wang, L. Dong, Y.H. Hu, G.S. Zheng, Z. Hu, Y. Chen, *J. Solid State Chem.* 157 (2001) 274–282.
- [35] G.M. Dhar, B.N. Srinivas, M.S. Rana, M. Kumar, S.K. Maity, *Catal. Today* 86 (2003) 45–60.
- [36] D. Zhao, C. Chen, Y. Wang, W. Ma, J. Zhao, T. Rajh, L. Zang, *Environ. Sci. Technol.* 42 (2008) 308–314.
- [37] C. Pophal, F. Kameda, K. Hoshino, S. Yoshinaka, K. Segawa, *Catal. Today* 39 (1997) 21–32.
- [38] G.W. Chen, S.L. Li, F.J. Jiao, Q. Yuan, *Catal. Today* 125 (2007) 111–119.
- [39] M.E. Manriquez, T. Lopez, R. Gomez, J. Navarrete, *J. Mol. Catal. A: Chem.* 220 (2004) 229–237.
- [40] V. Vishwanathan, H.S. Roh, J.W. Kim, K.W. Jun, *Catal. Lett.* 96 (2004) 23–28.
- [41] K. Tanabe, M. Misono, Y. Ono, H. Hattori, Elsevier Science Ltd (1990).
- [42] R. Linacero, M.L. Rojas-Cervantes, J.D.D. Lopez-Gonzalez, *J. Mater. Sci.* 35 (2000) 3279–3287.
- [43] S.D. Yim, I.S. Nam, *J. Catal.* 221 (2004) 601–611.
- [44] J. Ramirez, A. Gutierrez Alejandro, *J. Catal.* 170 (1997) 108–122.
- [45] W.F. Yan, Z. Ma, S.M. Mahurin, J. Jiao, E.W. Hagaman, S.H. Overbury, S. Dai, *Catal. Lett.* 121 (2008) 209–218.
- [46] E. Olguin, M. Vrinat, L. Cedeno, J. Ramirez, M. Borque, A. Lopez-Agudo, *Appl. Catal. A: Gen.* 165 (1997) 1–13.
- [47] G.A.M. Hussein, N. Sheppard, M.I. Zaki, R.B. Fahim, *J. Chem. Soc., Faraday Trans.* 87 (1991) 2655–2659.
- [48] R. Peters, H.G. Dusterwald, B. Hohlein, *J. Power Sources* 86 (2000) 507–514.
- [49] J.P. Breen, F.C. Meunier, J.R.H. Ross, *Chem. Commun.* (1999) 2247–2248.
- [50] I.A. Fisher, A.T. Bell, *J. Catal.* 184 (1999) 357–376.
- [51] D. Chadwick, K.G. Zheng, *Catal. Lett.* 20 (1993) 231–242.